Korean J. Chem. Eng., **30**(3), 724-732 (2013)
DOI: 10.1007/s11814-012-0187-9

Modeling interfacial tension of $(CH_4+N_2)+H_2O$ and $(N_2+CO_2)+H_2O$ systems using linear gradient theory

Shahin Khosharay and Farshad Varaminian†

School of Chemical, Gas and Petroleum Engineering, Semnan University, Iran
(*Received 6 July 2012 • accepted 3 November 2012*)

Abstract−The linear gradient theory (LGT) of fluid interfaces in combination with the cubic-plus-association equation of state (CPA EOS) is applied to determine the interfacial tensions of $(CH_4+N_2)+H_2O$ and $(N_2+CO_2)+H_2O$ ternary mixtures from 298-373 K and 10-300 bar. First, the pure component influence parameters of CH_4, N_2, CO_2 and H_2O are obtained. Then, temperature-dependent expressions of binary interaction coefficient for (CH_4+H_2O), (N_2+H_2O) and (CO_2+H_2O) are correlated. These empirical correlations of pure component influence parameters and binary interaction coefficients are applied for ternary mixtures. For $(CH_4+N_2)+H_2O$ and $(N_2+CO_2)+H_2O$ mixtures, the predictions show good agreement with experimental data (overall AAD~1.31%).

Key words: Interfacial Tension, CPA Equation of State, Linear Gradient Theory, Ternary Mixtures

INTRODUCTION

Interfacial tension is a basic but often overlooked thermophysical property that plays a major role in chemistry and chemical engineering applications, including extraction, distillation, gas absorption, heat transfer under boiling conditions, and mass transfer during extraction. In the petroleum industry, in particular in the exploration, production and processing of petroleum fluids, interfacial tension must be accurately determined because it has a dominant influence on capillary pressure, relative permeability and residual liquid saturation [1,2]. The interfacial tension of gas/water mixtures plays an important role in many processes; for example, the nucleation of hydrate depends on the interfacial phenomenon, so interfacial properties such as the interfacial tension of gas/water may have a great influence upon the hydrate formation rate [3,4].

Although measurements of interfacial tensions are of interest, available experimental data are insufficient. Thus, using a reliable method that provides accurate estimations of interfacial tensions is of importance. Several attempts have been made to correlate and predict the interfacial tension of pure fluids and mixtures that range from simple empirical correlations to methods based on statistical thermodynamics. The parachor method [5-8] and its derivatives is the most basic one. The corresponding states principle [9-12], perturbation theory [13,14], density functional theory [15-19] and gradient theory [2] are the other approaches for describing interfacial tension of pure fluids and mixtures.

The gradient theory of inhomogeneous fluid is a robust method for describing the interfacial tension of pure fluids and mixtures. This theory originated in the work of van der Waals [20]. Cahn and Hilliard [21] reformulated this theory in 1958. It can be applied to a wide range of fluids: hydrocarbons and their mixtures [22-25], polar compounds and their mixtures [26,27], polymer and polymer melts [28-31], near-critical interfaces [32-35] and other liquid-liquid interfaces [36]. The only inputs required for the gradient theory are the Helmholtz free energy density of the homogeneous fluid and the influence parameter of the inhomogeneous fluid. The Helmholtz free energy density can be calculated by using any thermodynamic model, and the influence parameter has a molecular-theoretical basis. This definition is too difficult to be applied in practice. One way to overcome this problem is, for instance, to use a semi-empirical expression [37].

Carey et al. [24,38] used the coupling of the gradient theory with cubic equations of state (EOSs) to determine the interfacial tension of pure fluids and mixtures. They also proposed a semi-empirical influence parameter correlation to determine the interfacial tension. Schmidt et al. [2] combined the linear gradient theory (LGT) with the SRK and PR EOSs to estimate the interfacial tensions of the methane-water system. They also found the influence parameters of both methane and water and binary interaction coefficient for the mixture influence parameter. Lafitte et al. [39] used gradient theory of fluid interfaces in combination with SAFT-VR Mie EOS to determine the interfacial properties of the water/CO_2 mixture. The results of simulation were in good agreement with experimental data. Mejýa et al. [40] applied the gradient theory (GT) in combination with the global phase diagram approach (GPDA) to predict the interfacial tension of mixtures with no need for experimental data. The results of this model predicted the interfacial tensions in satisfactory manner. Mejıa et al. [41] combined the gradient theory with an improved Peng-Robinson equation of state to predict interfacial tensions of miscible mixtures. To demonstrate the potential of this method, the results for subcritical binary mixtures are compared to experimental data and the Parachor method. Miqueu et al. [42] simultaneously applied the gradient theory and Monte Carlo simulation to determine interfacial behavior of a methane-water mixture. Both methods provided very good estimations of the interfacial behavior of mixture and results of both simulations were the same as each other.

In this paper, the linear gradient theory (LGT) in combination with cubic-plus-association equation of state (CPA EOS) is used to

†To whom correspondence should be addressed.
E-mail: fvaraminian@semnan.ac.ir

determine the interfacial tensions of pure fluids and mixtures. A temperature-dependent correlation of the influence parameters is performed to predict the interfacial tension of pure fluids (CH_4, N_2, CO_2 and H_2O) and mixtures. Then the interfacial tensions of (N_2+H_2O), (CH_4+H_2O) and (CO_2+H_2O) binary systems are modeled and the binary interaction coefficients of influence parameter are fitted. Interfacial tensions of (CH_4+N_2)+H_2O and (CO_2+N_2)+H_2O systems at different temperatures, pressures and compositions are determined by applying the linear gradient theory (LGT). The calculation results show good agreement with experimental data.

MODEL

1. Linear Gradient Theory

Gradient theory has been described extensively in numerous investigations [2,42-45]. According to the gradient theory, the interfacial tension of the planar interface can be computed with:

$$\gamma = \int_{\rho_{ref}^{V}}^{\rho_{ref}^{L}} \sqrt{2(\Omega(\rho) - \Omega_B)\sum_i\sum_j \kappa_{ij}\frac{d\rho_i}{d\rho_{ref}}\frac{d\rho_j}{d\rho_{ref}}}\, d\rho_{ref} \tag{1}$$

in which Ω_B=−P and P is an equilibrium pressure, ρ the mole density, γ the interfacial tension, subscript ref the reference component, $d\rho_i/d\rho_{ref}$ the mole density profile for component i and κ is the influence parameter. ρ^L and ρ^V represent the liquid and vapor bulk phases mole densities, respectively. $\Omega(\rho)$ is the grand thermodynamic potential computed as follows:

$$\Omega(\rho) = f_0(\rho) - \sum_i \rho_i \mu_{is} \tag{2}$$

in which $f_0(\rho)$ denotes the Helmholtz free energy density of the homogeneous fluid at local mole density of ρ, and μ_{is} denotes the chemical potential of component i in the bulk phase.

Zuo and Stenby [46,47] proposed the linear gradient theory (LGT) in which it is unnecessary to solve the set of density profile equations that are inherent in the gradient theory model. It simplified the calculation procedure without significantly losing accuracy for results of modeling. The linear gradient theory assumes that $\rho_i(z)$−ρ_i at the position z on the interface with width h is linearly distributed across the interface.

$$\frac{d\rho_i(z)}{dz} = D_i \tag{3}$$

$$D_i = \frac{\Delta\rho_i}{h} = \frac{\rho_i^{II} - \rho_i^{I}}{h} \tag{4}$$

D_i is a constant for each component i. ρ_i^I and ρ_i^{II} show the density of component i at the boundary conditions (the coexisting equilibrium phases).

Similar to the gradient theory, the interfacial tension can be determined with:

$$\gamma = \int_{\rho_1^I}^{\rho_1^{II}} \sqrt{2\kappa(\Omega(\rho) - \Omega_B)}\, d\rho_1 \tag{5}$$

in which κ is the mixture influence parameter.

Subscript 1 represents the component with the maximum density difference between the two homogenous phases (coexisting phases I and II).

$$\Delta\rho_1 = \max(\rho_i^I - \rho_i^{II}) \quad i = 1,\ldots,N_c \tag{6}$$

According to Zuo and Stenby [46], the influence parameter can be determined with:

$$\kappa = \sum_i\sum_j \kappa_{ij}\frac{\Delta\rho_i}{\Delta\rho_1}\frac{\Delta\rho_j}{\Delta\rho_1} \tag{7}$$

or [47]:

$$\kappa = \sum_i\sum_j \kappa_{ij} x_i x_j \tag{8}$$

in which x_i is the mole fraction of component i in the liquid phase.

The crossed influence parameters κ_{ij} is calculated by:

$$\kappa_{ij} = \sqrt{\kappa_i\kappa_j}(1 - l_{ij}) \tag{9}$$

in which κ_i, κ_j and l_{ij} are the influence parameters of the pure i and j components and binary interaction coefficient, respectively.

2. CPA Equation of State

We used the CPA equation of state to determine the mole densities of the bulk phases and the Helmholtz free energy density. The CPA equation shows good performance in predicting the liquid and vapor densities of gas/water mixtures.

For the compressibility factor, the CPA equation of state combines two contributions: one part that accounts for physical interactions between molecules (the Soave-Redlich-Kwong (SRK) EOS), and a second part that accounts for the association between molecules (the Wertheim association theory [48]).

$$Z = Z^{phys.} + Z^{assoc.} = \frac{1}{1-b\rho} - \frac{a\rho}{RT(1+b\rho)} - \frac{1}{2}\left(1 + \rho\frac{\partial \ln g}{\partial\rho}\right)\sum_i x_i \sum_{A_i}(1 - X_{A_i}) \tag{10}$$

where a is the energy parameter, b is the co-volume parameter, ρ is the mole density, g is the simplified radial distribution function [49], X_{A_i} is the mole fraction of pure component i (not bonded at site A), and x_i is the mole fraction of component i.

X_{A_i} is an important component of the association term and is solved by the following equation:

$$X_{A_i} = \frac{1}{1 + \rho\sum_j x_j \sum_i X_{B_j}\Delta^{A_iB_j}} \tag{11}$$

The term $\Delta^{A_iB_i}$ (for self-associating molecules) is given by the following expression:

$$\Delta^{A_iB_i} = g(\rho)\left[\exp\left(\frac{\varepsilon^{A_iB_i}}{RT}\right) - 1\right] b_{ii}\beta^{A_iB_i} \tag{12}$$

where $\varepsilon^{A_iB_i}$ and $\beta^{A_iB_i}$ are the association energy and volume, respectively. The Elliot combining rule is used for sites with two different associating molecules:

$$\Delta^{A_iB_j} = \sqrt{\Delta^{A_iB_i}\Delta^{A_jB_j}} \tag{13}$$

The simplified expression for the hard-sphere radial distribution $g(\rho)$ is given by the following equation:

$$g(\rho) = \frac{1}{1 - 1.9\eta}, \quad \eta = \frac{1}{4}b\rho \tag{14}$$

The calculation procedure of pure-compound parameters of CPA

EOS is presented in [50]. For CH_4, CO_2 and N_2, the CPA EOS reduces to the SRK EOS. A four-site (4C) association scheme is used for water within the CPA framework:

$$X_A = X_B = X_C = X_D = \frac{-1+\sqrt{1+8\rho\Delta^{AC}}}{4\rho\Delta^{AC}} \quad (15)$$

$$\Delta^{AA}=\Delta^{AB}=\Delta^{BB}=\Delta^{CC}=\Delta^{CD}=\Delta^{DD}=0$$
$$\Delta^{AC}=\Delta^{AD}=\Delta^{BC}=\Delta^{BD}\neq 0 \quad (16)$$

The classical van der Waals mixing rule is used to calculate the vapor-liquid equilibrium according to the following expressions:

$$a = \sum_i \sum_j a_{ij} x_i x_j \quad (17)$$

$$a_{ij} = \sqrt{a_i a_j}(1-k_{ij}) \quad (18)$$

$$b = \sum_i b_i x_i \quad (19)$$

In Eqs. (17-19), x_i is the mole fraction of each component i in each phase, and k_{ij} is the binary interaction parameter. The following temperature-dependent binary interaction parameters [50] in the range of 273.15 K up to 393.15 K are used:

$$k_{CH_4\text{-}H_2O} = 0.8613 - \frac{251.0540}{T/K} \quad (20)$$

$$k_{N_2\text{-}H_2O} = 0.9909 - \frac{379.9691}{T/K} \quad (21)$$

$$k_{CO_2\text{-}H_2O} = 0.1099 - \frac{53.7586}{T/K} \quad (22)$$

The results of calculation in ref [50] indicated that the predicted gas solubilities by the CPA EOS are in a good agreement with the experimental data even for supercritical phase equilibrium of mixtures. The binary interaction parameters (k_{ij}) of CH_4-N_2, N_2-CO_2 and CH_4-CO_2 are set equal to zero.

3. The Influence Parameters of Pure Fluids

The influence parameters of pure fluids (CH_4, N_2, CO_2 and H_2O) are determined by correlations to interfacial tension data:

Table 1. Correlation coefficients for the influence parameters calculation

Fluid	$A\times10^{16}$	$B\times10^{16}$	$C\times10^{16}$	T_r range	%AAD	γ_{exp} Ref.
C_1	0.78861	−1.46447	1.22010	0.47-0.94	0.66	[51]
N_2	0.48456	2.21481	1.51172	0.62-0.95	0.76	[51]
CO_2	0.84676	−1.38573	0.99824	0.71-0.99	0.60	[51]
H_2O	−0.45479	−1.02970	2.31771	0.42-0.99	0.88	[51]

Table 2. Measured and calculated interfacial tensions for CH_4/H_2O mixture

P (bar)	298.15 K γ(mN·m^{-1})		313.15 K γ(mN·m^{-1})		333.15K γ(mN·m^{-1})		353.15K γ(mN·m^{-1})		373.15K γ(mN·m^{-1})		γ_{exp} Ref.
	Calc	Exp	Calc	Exp	Calc	Exp	Calc	Exp	Calc	Exp	
10	71.02	72.96	68.66	69.06	65.41	66.29	62.03	62.65	58.59	59.77	[52]
50	67.31	68.32	65.13	65.85	62.31	62.82	59.35	59.56	56.23	56.09	[52]
100	62.78	63.86	60.89	61.77	58.66	59.45	56.31	56.79	53.73	53.95	[52]
150	58.92	59.71	57.23	57.89	55.50	55.86	53.71	53.79	51.62	52.00	[52]
200	56.14	56.14	54.44	54.14	53.85	53.01	51.64	51.70	49.94	49.83	[52]
300	53.07	52.42	51.10	50.82	49.83	49.66	48.89	48.59	47.75	47.75	[52]
%AAD	0.80										

Table 3. Measured and calculated interfacial tensions for N_2/H_2O mixture

P (bar)	298.15 K γ(mN·m^{-1})		313.15 K γ(mN·m^{-1})		333.15K γ(mN·m^{-1})		353.15K γ(mN·m^{-1})		373.15K γ(mN·m^{-1})		γ_{exp} Ref.
	Calc	Exp	Calc	Exp	Calc	Exp	Calc	Exp	Calc	Exp	
10	71.41	71.43	69.02	69.36	65.70	65.68	62.24	62.17	58.73	58.03	[53]
30	70.42	70.45	68.02	68.26	64.75	64.94	61.32	61.43	57.80	57.00	[53]
50	69.47	69.23	67.08	67.25	63.87	64.28	60.49	60.43	56.89	56.10	[53]
100	67.37	67.21	64.98	65.05	61.90	62.74	58.62	58.66	55.09	54.25	[53]
150	65.64	65.54	63.24	63.32	60.24	60.85	57.05	57.3	53.88	53.76	[53]
200	64.25	63.94	61.83	61.66	58.90	59.44	55.74	55.57	52.68	52.37	[53]
250	63.14	63.15	60.71	60.55	57.80	57.8	54.67	54.67	51.67	51.66	[53]
300	62.28	62.66	59.81	59.82	56.92	56.41	53.79	53.66	50.85	51.11	[53]
%AAD	0.46										

$$\kappa = \frac{1}{2}\left[\frac{\gamma_{exp}}{\int_{\rho^l}^{\rho^v}\sqrt{f_0(\rho)-\rho\mu(\rho)+P}\,d\rho}\right]^2 \quad (23)$$

For interfacial tensions, deviations are given by:

$$AAD_\gamma = \frac{1}{N}\sum_{i=1}^{N}\left|\frac{\gamma_i^{exp}-\gamma_i^{calc}}{\gamma_i^{exp}}\right| \quad (24)$$

In Eq. (24), N represents the number of experimental points. The experimental interfacial tensions are presented in Baidakov et al. [51]. Similar to expression of Oliveira et al. [48] for influence parameters, the influence parameters of pure fluids are determined as a function of the reduced temperature.

$$\frac{\kappa}{ab^{2/3}} = A.(1-T_r)^2 + B.(1-T_r) + C \quad (25)$$

A, B and C are the correlation coefficients listed in Table 1.

Table 4. Measured and calculated interfacial tensions for CO_2/H_2O mixture

P (bar)	T (k)	γ(mN·m^{-1})		γ_{exp} Ref.	P (bar)	T (k)	γ(mN·m^{-1})		γ_{exp} Ref.
		Calc	Exp				Calc	Exp	
10.1	297.8	63.93	65.73±0.27	[54]	600.0	333.5	20.88	19.72±0.03	[54]
20.0	297.9	57.37	58.90±0.21	[54]	10.0	343.3	59.84	61.28±0.53	[54]
30.0	297.9	51.77	52.42±0.36	[54]	20.0	343.3	56.03	57.00±0.27	[54]
40.0	297.9	47.01	47.02±0.32	[54]	30.0	343.3	53.09	55.58±0.38	[54]
50.1	297.9	42.92	41.29±0.20	[54]	40.0	343.3	48.94	51.55±0.17	[54]
60.1	297.9	39.48	36.00±0.24	[54]	50.0	343.3	46.18	48.50±0.20	[54]
70.2	297.9	31.06	30.12±0.11	[54]	60.0	343.3	43.77	45.36±0.23	[54]
80.2	297.9	30.28	30.28±0.08	[54]	70.5	343.3	41.59	42.49±0.18	[54]
100.1	297.9	29.19	29.66±0.20	[54]	80.3	343.3	39.84	39.83±0.30	[54]
149.9	297.9	27.49	27.73±0.10	[54]	90.2	343.3	38.32	37.46±0.17	[54]
199.9	279.9	26.38	25.99±0.09	[54]	100.3	343.3	36.99	35.38±0.25	[54]
10.0	312.9	62.31	63.55±0.26	[54]	110.4	343.3	35.88	33.97±0.16	[54]
19.9	312.8	57.30	58.79±0.27	[54]	120.5	343.3	34.91	32.75±0.19	[54]
29.9	312.8	51.20	51.15±0.11	[54]	150.9	343.3	32.45	30.31±0.15	[54]
40.1	312.8	46.80	46.94±0.27	[54]	202.0	343.3	29.44	28.36±0.12	[54]
50.2	312.8	43.15	43.93±0.23	[54]	252.5	343.3	27.44	27.46±0.08	[54]
60.0	312.8	40.22	40.21±0.17	[54]	352.8	343.3	24.86	25.52±0.12	[54]
70.2	312.9	35.76	36.87±0.19	[54]	413.2	343.3	23.78	24.41±0.14	[54]
80.2	312.9	33.50	33.47±0.19	[54]	10.0	374.3	55.97	56.20±0.50	[54]
100.0	312.9	32.40	31.20±0.15	[54]	20.0	374.3	52.95	53.44±0.40	[54]
150.0	312.9	29.19	29.17±0.13	[54]	30.0	374.3	50.27	51.23±0.25	[54]
200.2	312.2	27.52	28.33±0.16	[54]	40.0	374.3	47.88	48.76±0.08	[54]
249.92	312.9	26.32	27.14±0.09	[54]	50.0	374.3	45.72	46.23±0.09	[54]
10.0	333.5	61.65	62.48±0.33	[54]	60.0	374.3	43.78	44.64±0.13	[54]
19.9	333.5	57.67	59.93±0.40	[54]	90.0	374.3	39.03	39.67±0.04	[54]
29.9	333.5	54.10	56.03±0.26	[54]	100.0	374.3	37.75	38.05±0.25	[54]
39.9	333.5	50.93	52.42±0.25	[54]	110.0	374.3	36.60	36.64±0.16	[54]
50.0	333.5	48.09	49.49±0.22	[54]	120.0	374.3	35.55	35.05±0.37	[54]
60.0	333.5	45.59	46.28±0.15	[54]	130.0	374.3	34.61	33.81±0.50	[54]
70.1	333.5	43.35	43.36±0.12	[54]	140.0	374.3	33.74	32.81±0.32	[54]
80.1	333.5	41.39	40.49±0.08	[54]	150.0	374.3	32.95	32.22±0.37	[54]
89.9	333.5	38.67	37.76±0.18	[54]	160.0	374.3	32.21	31.21±0.39	[54]
100.0	333.6	33.21	32.05±0.27	[54]	170.0	374.3	31.51	30.45±0.23	[54]
105.7	333.6	32.02	31.23±0.24	[54]	180.0	374.3	30.86	29.92±0.26	[54]
150.1	333.5	31.07	30.47±0.15	[54]	190.0	374.3	30.26	29.27±0.34	[54]
200.0	333.5	29.09	29.07±0.07	[54]	200.0	374.3	29.68	29.13±0.17	[54]
250.0	333.5	27.27	27.44±0.17	[54]	300.0	374.3	25.25	25.27±0.13	[54]
300.0	333.5	25.98	26.91±0.12	[54]	400.0	374.3	22.48	24.04±0.10	[54]
400.0	333.5	24.18	24.81±0.11	[54]	499.9	374.3	21.57	22.25±0.11	[54]
500.0	333.5	22.96	22.97±0.16	[54]	600.5	374.3	20.19	21.23±0.04	[54]
%AAD					1.98				

CALCULATION RESULTS

1. Binary Mixtures

The simplification of the linear gradient theory is in principle unsuitable for (gas+water) mixtures because gases adsorb at the interface, and this behavior cannot be reproduced by the linear gradient theory (LGT). For suitable prediction of interfacial tension of these kinds of mixtures binary interaction coefficient should be determined by fitting the experimental interfacial tensions of binary systems. The binary interaction coefficient is found to be dependent on the temperature, so it is necessary to determine temperature-dependent binary interaction coefficient (l_{ij}). The experimental [52,53] and calculated interfacial tensions for the (N_2+H_2O), (CH_4+H_2O) and (CO_2+H_2O) binary mixtures are presented at various pressures and temperatures in Tables 2-4 and Figs. 1-3. To demonstrate the central hypothesis of their approach, first the binary coefficient of the influence parameter was set to zero (l_{ij}=0). The results (Figs. 1-3) indicate that the hypothesis of linear density profiles is not reliable for N_2/H_2O, CO_2/H_2O and CH_4/H_2O systems in the temperature range

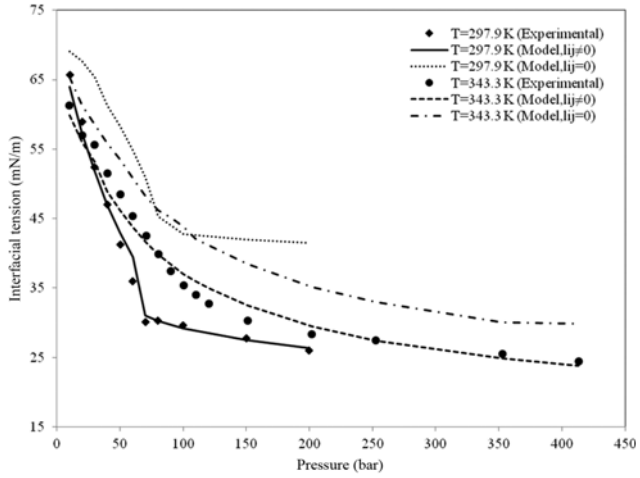

Fig. 1. Plot of calculated and experimental interfacial tensions of (CO_2+H_2O) versus the pressure at 297.9 K and 343.3 K.

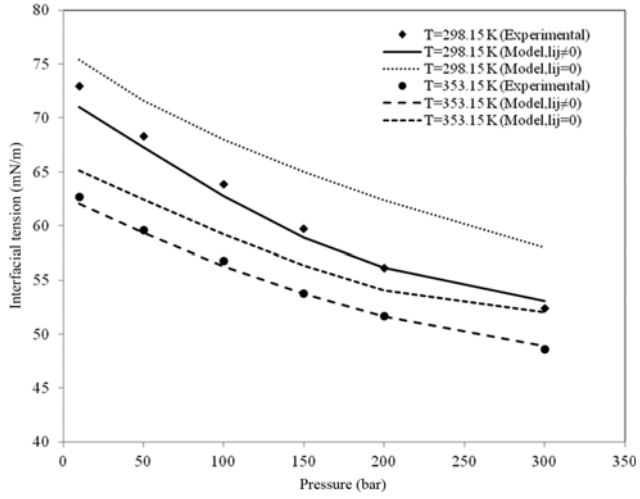

Fig. 2. Plot of calculated and experimental interfacial tensions of (CH_4+H_2O) versus the pressure at 298.15 K and 353.15 K.

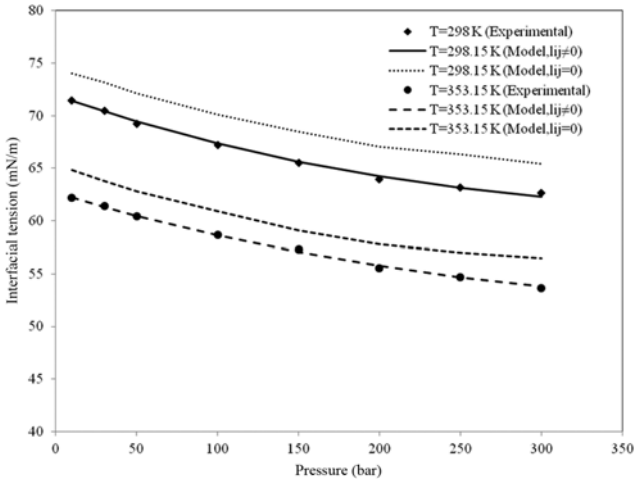

Fig. 3. Plot of calculated and experimental interfacial tensions of (N_2+H_2O) versus the pressure at 298.15 K and 353.15 K.

of (298-373) K and pressure range of (10-300). So, the correlations with the LGT model for determination of l_{ij} should be done because the linear assumption of densities across the interfacial region is inadequate.

The binary interaction coefficients of these binary mixtures are fitted for all of the experimental data (isotherms). The following temperature-dependent expressions are correlated for l_{ij}:

$$l_{H_2O,N_2} = 2.2790 - 0.00457\,T/K \quad (26)$$

$$l_{H_2O,CH_4} = 0.696 - 0.000562\,T/K \quad (27)$$

$$l_{H_2O,CO_2} = -0.591 + 0.00712\,T/K \quad (28)$$

Two isotherms (297.9 and 343.3 K) are plotted in Fig. 1 together with the calculated interfacial tensions for (CO_2+H_2O) mixture. For these two isotherms, one can observe abrupt change in slope (two distinct regions). The pressure-dependence of interfacial tension can be related to the isothermal compressibility (β) of phases. The intersection points of these two regions are the pressures at which the compressibility of pure CO_2 is maximized at each temperature. At temperatures below CO_2 critical temperature (T=297.9 K), β_{max} corresponds to the phase change of equilibrium from vapor-liquid equilibrium (VLE) at low pressures to liquid-liquid equilibrium (LLE) at high pressures. For temperature above the critical temperature of CO_2 (T=343.3 K), β_{max} corresponds to change from vapor CO_2/liquid water to supercritical CO_2/liquid water. Water is virtually incompressible. The CO_2 compressibility directly influences the free energy density and therefore the interfacial tension of mixture [39,54]. The present model satisfactorily reproduces the interfacial tensions of CO_2/H_2O binary mixture and the pressure-dependence of interfacial tensions of this mixture. Similar results are also observed for the N_2/H_2O system. The pressure-dependence of interfacial tension for CH_4/H_2O system is relatively simple, with a slightly steeper slope at the lower pressures.

2. Ternary Mixtures

In the previous section, the results obtained for the binary mixtures prove that the linear gradient theory (LGT) works well for these mixtures. Hence, the linear gradient theory (LGT) model can be applicable to the ternary mixtures. The experimental interfacial ten-

sions of ternary mixtures are taken from Yan et al. [53], who measured the interfacial tensions by using the pendant-drop method. The temperature and pressure are in the range of (298-373) K and (10-300) bar, respectively. To determine quality of the prediction of the phase equilibrium data for the ternary system, the density difference between the two phases (liquid and vapor) is calculated with CPA EOS. The results of calculations are compared with experimental data in [53]. With an overall AAD of 3.85% for the density difference between the two phases, CPA EOS allows good predictions for the phase equilibrium data. Table 5 shows the experimen-

Table 5. Measured and calculated interfacial tensions for $(CH_4+N_2)+H_2O$ and $(N_2+CO_2)+H_2O$ mixtures

P (bar)	298.15 K γ(mN·m^{-1})		313.15 K γ(mN·m^{-1})		333.15 K γ(mN·m^{-1})		353.15 K γ(mN·m^{-1})		373.15 K γ(mN·m^{-1})		γ_{exp} Ref.
	Calc	Exp	Calc	Exp	Calc	Exp	Calc	Exp	Calc	Exp	
(23.64 mol% CH_4+76.36 mol% N_2)+H_2O											
10	71.32	71.28	68.93	68.78	65.63	65.62	62.19	62.01	58.69	58.33	[53]
30	70.14	69.71	67.76	68.02	64.54	64.68	61.17	60.81	57.70	57.01	[53]
50	69.01	68.80	66.59	67.20	63.52	63.71	60.23	60.29	56.85	56.18	[53]
100	66.45	66.33	64.14	64.76	61.21	61.30	58.13	58.13	54.97	54.41	[53]
150	64.33	64.41	62.04	62.93	59.27	59.40	56.34	56.21	53.40	53.18	[53]
200	62.63	62.95	60.34	60.77	57.68	58.39	54.87	55.05	52.08	51.99	[53]
300	60.30	60.29	57.95	58.46	55.38	55.54	52.70	52.92	50.13	50.49	[53]
%AAD	0.26		0.78		0.34		0.28		0.76		
(50.09 mol% CH_4+49.01 mol% N_2)+H_2O											
10	71.43	71.12	69.06	68.80	65.76	65.78	62.34	61.90	58.84	58.06	[53]
30	70.26	69.80	67.92	67.82	64.76	64.58	61.46	60.89	58.01	56.90	[53]
50	69.05	68.76	66.75	66.79	63.72	63.49	60.56	60.04	57.24	56.02	[53]
100	66.21	65.91	64.01	64.20	61.25	61.75	58.41	57.68	55.44	53.94	[53]
150	63.81	63.12	61.66	61.54	59.13	59.05	56.56	55.58	53.85	52.46	[53]
200	62.01	61.00	59.79	59.04	57.46	57.28	55.03	54.34	52.57	51.19	[53]
300	59.76	57.96	57.44	56.45	55.17	54.02	52.94	51.64	50.82	49.17	[53]
%AAD	1.18		0.58		0.58		1.33		2.42		
(74.93 mol% CH_4+25.07 mol% N_2)+H_2O											
10	71.12	71.30	68.75	68.72	65.48	65.32	62.09	62.01	58.61	58.03	[53]
30	69.50	69.70	67.19	67.39	64.08	64.10	60.83	60.84	57.46	57.02	[53]
50	67.91	68.05	65.67	65.84	62.73	63.08	59.66	59.54	56.44	55.98	[53]
100	64.15	64.77	62.08	62.55	59.58	60.10	56.96	57.24	54.17	54.00	[53]
150	60.98	61.42	59.03	60.13	56.88	57.71	54.65	55.23	52.25	52.18	[53]
200	58.56	58.97	56.62	57.58	54.71	55.63	52.78	53.41	50.69	50.78	[53]
300	55.59	54.98	53.51	53.66	51.78	52.50	50.20	50.62	48.54	48.54	[53]
%AAD	0.60		0.73		0.88		0.55		0.46		
(24.97 mol% CO_2+75.03 mol% N_2)+H_2O											
10	69.63	69.33	67.38	67.95	64.72	64.90	61.37	61.74	58.09	58.32	[53]
50	62.31	60.47	60.42	59.72	59.64	58.71	56.63	56.34	53.98	54.21	[53]
100	56.24	53.44	54.49	53.25	54.90	52.78	52.16	51.23	50.08	50.01	[53]
150	52.37	49.78	50.58	49.37	51.46	49.22	48.84	47.87	47.08	47.49	[53]
200	49.88	47.71	47.99	47.64	48.95	47.02	46.37	46.09	44.78	45.47	[53]
300	47.05	45.30	45.01	45.05	45.74	44.31	43.13	43.21	41.62	41.64	[53]
%AAD	3.72		1.29		2.96		0.95		0.56		
(50.72 mol% CO_2+49.28 mol% N_2)+H_2O											
10	67.76	67.96	65.69	66.29	63.70	63.96	60.47	60.50	57.41	57.15	[53]
50	55.58	56.10	54.25	55.60	55.57	54.83	52.95	53.30	51.04	51.46	[53]
100	47.00	46.65	45.96	47.24	48.74	47.68	46.56	46.79	45.41	45.35	[53]
150	42.75	41.58	41.63	42.33	44.40	42.83	42.39	41.86	41.52	40.92	[53]
200	40.65	40.07	39.42	40.12	41.63	40.24	39.68	38.87	38.81	37.87	[53]
300	38.61	37.66	37.40	36.86	37.08	36.18	36.64	34.77	35.51	33.61	[53]
%AAD	1.45		1.81		2.26		1.65		1.83		

Table 5. Continued

P (bar)	298.15 K γ(mN·m^{-1})		313.15 K γ(mN·m^{-1})		333.15 K γ(mN·m^{-1})		353.15 K γ(mN·m^{-1})		373.15 K γ(mN·m^{-1})		γ_{exp} Ref.
	Calc	Exp	Calc	Exp	Calc	Exp	Calc	Exp	Calc	Exp	
(75.85 mol% CO_2+24.15 mol% N_2)+H_2O											
10	65.60	65.85	64.00	64.74	62.68	62.92	59.58	59.33	56.75	55.97	[53]
50	49.22	49.63	48.62	51.20	51.74	52.02	49.54	51.47	48.29	49.09	[53]
100	35.82	37.24	39.20	40.96	43.34	43.09	41.80	42.75	41.36	41.84	[53]
150	32.83	33.08	35.94	35.74	38.70	38.47	37.42	37.74	36.99	36.97	[53]
200	31.35	31.88	34.52	33.69	36.10	35.18	34.91	34.10	34.22	33.72	[53]
300	32.53	32.72	32.63	32.83	33.21	33.51	32.13	30.33	30.96	29.23	[53]
%AAD	1.33		2.35		0.93		2.59		1.93		
Avragel %AAD	1.31										

tal data and the results of calculations for the (CH_4+N_2)+H_2O and (N_2+CO_2)+H_2O in the temperature range of (298-373) K and the pressure range of (10-300) bar. Figs. 4 and 5 compare the results of model with the data of Yan et al. [53].

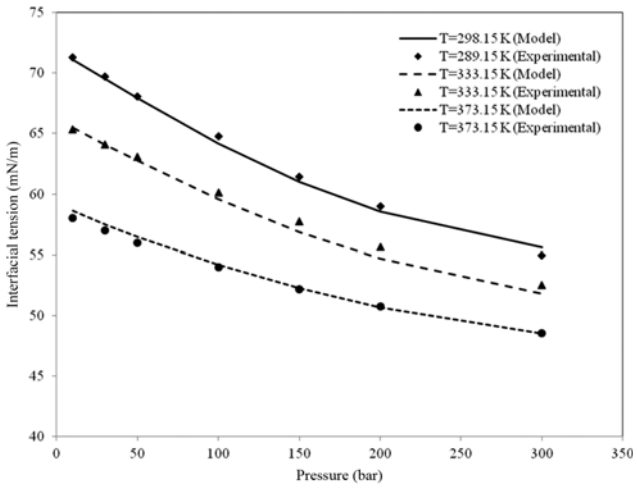

Fig. 4. Plot of surface tension versus pressure for the (74.93 mol% CH_4+25.07 mol% N_2)+H_2O mixture at 298.15 K, 333.15 K and 373.15 K.

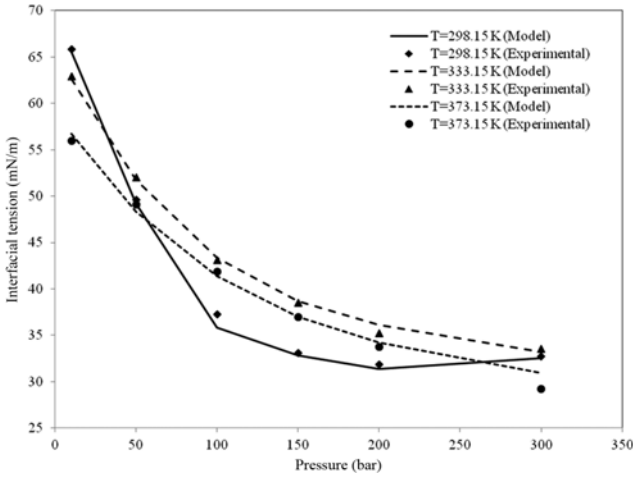

Fig. 5. Plot of surface tension versus pressure for the (75.85 mol% CO_2+24.15 mol% N_2)+H_2O mixture at 298.15 K, 333.15 K and 373.15 K.

The pressure, temperature and composition dependence of the interfacial tension of (CH_4+N_2)+H_2O is relatively simple. At fixed gas composition and temperature, one can see the decrease of interfacial tension with increasing pressure with little different slopes at lower and higher pressures. At fixed gas composition and pressure, one can see decrease in interfacial tension with increasing temperature. At fixed pressure and temperature, increase in methane content lead to decrease in interfacial tension [53]. The present model fairly reproduces this behavior.

For (CO_2+N_2)+H_2O, pressure, temperature and composition dependence of the interfacial tension is almost the same as (CO_2+N_2)+H_2O except for high concentration of CO_2 (75.84 mol%). The interfacial tension-pressure isotherm has a minimum at ~200 bar [53]. The present model also reproduces this minimum at ~200 bar.

The temperature dependence of interfacial tension of (CO_2+N_2)+H_2O system is different from (CH_4+N_2)+H_2O system. At low pressures, increase in temperature leads to decrease interfacial tension at fixed the composition, but because of different slopes of interfacial tension-pressure isotherms, some curves intersect each other at high pressures [53]. Except for T=313 K, the applied model fairly reproduces this complicated temperature dependence.

At fixed pressure and temperature, increase in nitrogen and carbon dioxide content results in decrease in interfacial tension. The applied model fairly predicts this behavior.

The overall %AAD in the interfacial tension is 1.31 for these two mixtures, which demonstrates that the current model is good for these two mixtures.

The main distinctions of the present model with respect to the previous works are:

• The linear gradient theory (LGT) of fluid interfaces in combination with cubic-plus-association equation of state (CPA EOS) is successfully used for determination of CO_2+H_2O and (N_2+CO_2)+H_2O interfacial tensions (To our knowledge, Yan et al. [53] did not successfully use the linear gradient theory for these two systems.).

• The present model successfully reproduces the pressure-dependence of CO_2/H_2O interfacial tension at different temperatures, whereas in some works such as that of Georgiadis et al. [54], more than one model was used for reproducing the pressure-dependence of CO_2/H_2O at different temperatures.

• The present model fairly predicts the complex temperature and pressure dependence of (N_2+CO_2)+H_2O mixture at high concentration of carbon dioxide (75.84 mol%).

CONCLUSIONS

The coupling of the linear gradient theory (LGT) with cubic-plus-association equation of state (CPA EOS) is applied to describe the interfacial tension of (CH_4+N_2)+H_2O and (N_2+CO_2)+H_2O ternary mixtures. This model successfully determines the pure component influence parameters for pure fluids (CH_4, N_2, CO_2 and H_2O). Then the temperature-dependent binary interaction coefficients for the influence parameters of (CH_4+H_2O), (N_2+H_2O) and (CO_2+H_2O) mixtures are successfully fitted. The predicted interfacial tensions of (CH_4+N_2)+H_2O and (N_2+CO_2)+H_2O ternary mixtures agree well with the experimental data. The present model also fairly predicts the complex temperature and pressure dependence of (CO_2+H_2O) and (N_2+CO_2)+H_2O.

NOMENCLATURE

a : attractive parameter in CPA EOS [Jm^3/mol^2]
AAD : average absolute deviation [%]
assoc : association part of CPA EOS
b : covolume in the EOS [m^3/mol]
B : bulk
calc : calculated result
D_i : the density gradient for component i
exp : experimental
f_0 : Helmholtz free energy density [J/m^3]
g : simplified radial distribution function
h : width of interface [m]
i, j : components i and j
k_{ij} : binary interaction parameter for the attractive parameter in the CPA EOS
L : liquid
l_{ij} : binary interaction coefficient for t he influence parameter of linear gradient theory
N : the number of experimental points
P : pressure [Pa]
phys : physical part of CPA EOS
R : ideal gas constant [$J\ mol^{-1}K^{-1}$]
ref : reference variable
T : temperature [K]
T_r : reduced temperature
V : vapor
x_i : mole fraction of each component i in each phase
X_A : fraction of molecule (not bonded at site A)
z : position in the interface [m]
Z : compressibility factor
β : isothermal compressibility [Pa^{-1}]
$\beta^{A_iB_i}$: the association volume
γ : interfacial tension [N/m]
ε : the association energy [J/mol]
Δ : association strength
η : reduced density
κ : influence parameter [$J\ m^5/mol^2$]
μ : chemical potential [J/mol]
ρ : mole density [mol/m^3]
Ω : grand thermodynamic potential [J/m^3]
I, II : coexisting phases I and II

REFERENCES

1. S. Y. Kim, S. S. Kim and B. Lee, *Korean J. Chem. Eng*., **26**, 349 (2009).
2. K. A. G. Schmidt, G. K. Folas and B. Kvamme, *Fluid Phase Equilib*., **261**, 230 (2007).
3. W. Yan, G.-Y., Zhao, G.-J. Chen and T. M. Guo, *J. Chem. Eng. Data*, **46**, 1544 (2001).
4. H. Luo, C. Y. Sun, Q. Huang, B. Z. Peng and G. J. Chen, *J. Colloid and Interface Sci*., **297**, 266 (2006).
5. D. B. Macleod, *Trans. Faraday Soc*., **19**, 38 (1923).
6. S. Sugden, *J. Chem. Soc. Trans*., **125**, 32 (1924).
7. S. Sugden, *J. Chem. Soc. Trans*., **125**, 1177 (1924).
8. C. F. Weinaug and D. L. Katz, *Ind. Eng. Chem*., **35**, 239 (1943).
9. E. A. Guggenheim, *J. Chem. Phys*., **13**, 253 (1945).
10. Y. X. Zuo and E. H. Stenby, *Can. J. Chem. Eng*., **75**, 1130 (1997).
11. A. J. Queimada, L. I. Rolo, A. I. Caco, I. M. Marrucho, E. H. Stenby and J. A. P. Coutinho, *Fuel*, **85**, 874 (2006).
12. A. J. Queimada, A. I. Caco, I. M. Marrucho and J. A. P. Coutinho, *J. Chem. Eng. Data*, **50**, 1043 (2005).
13. S. Toxvaerd, *J. Chem. Phys*., **57**, 4092 (1972).
14. J. M. Haile, C. G. Gray and K. E. Gubbins, *J. Chem. Phys*., **64**, 2569 (1976).
15. P. I. Teixeira and M. M. Telo da Gama, *J. Phys. Condens. Matter*., **3**, 111 (1991).
16. J. Winkelmann, *Ber. Bunsenges, Phys. Chem*., **98**, 1308 (1994).
17. J. Winkelmann, U. Brodrecht and I. Kreft, *Ber. Bunsenges. Phys. Chem*., **98**, 912 (1994).
18. D. Fu, J. F. Lu, J. C. Liu and Y. G. Li, *Chem. Eng. Sci*., **56**, 6989 (2001).
19. R. Evans, *Adv. Phys*., **28**, 143 (1979).
20. J. S. Rowlinson, *J. Stat. Phys*., **20**, 197 (1979).
21. J. W. Cahn and J. E. Hilliard, *J. Chem. Phys*., **28**, 258 (1958).
22. Y.-X. Zuo and E. H. Stenby, *Fluid Phase Equilib*., **132**, 139 (1997).
23. H. T. Davis and L. E. Stress, *Adv. Chem. Phys*., **49**, 357 (1982).
24. B. S. Carey, L. E. Scriven and H. T. Davis, *Am. Inst. Chem. Eng. J*., **24**, 1076 (1978).
25. H. T. Davis and L. E. Scriven, *Adv. Chem. Phys*., **49**, 357 (1982).
26. M. I. Guerrero, H. T. Davis, *Ind. Eng. Chem. Fundam*., **19**, 309 (1980).
27. H. Kahl and S. Enders, *Fluid Phase Equilib*., **172**, 27 (2000).
28. C. I. Poser and I. C. Sanchez, *J. Colloid Interface Sci*., **69**, 539 (1979).
29. G. T. Dee and B. B. Sauer, *J. Colloid Interface Sci*., **152**, 85 (1992).
30. B. B. Sauer and G. T. Dee, *J. Colloid Interface Sci*., **162**, 25 (1994).
31. H. S. Lee and W. H. Jo, *Polymer.*, **39**, 2489 (1998).
32. S. Fisk and B. Widom, *J. Chem. Phys*., **50**, 3219 (1969).
33. A. J. M. Yang, P. D. Fleming III and J. H. Gibbs, *J. Chem. Phys*., **64**, 3732 (1976).
34. S. Fisk and B. Widom, *J. Chem. Phys*., **50**, 3219 (1969).
35. P. M. W. Cornelisse, C. J. Peters and J. De Swann Arons, *Fluid Phase Equilib*., **117**, 312 (1996).
36. S. Enders and K. Quitzsch, *Langmuir*, **14**, 4606 (1998).

37. H. Lin, Y.-Y. Duan and Q. Min, *Fluid Phase Equilib*., **254**, 75 (2007).
38. B. S. Carey, L. E. Scriven and H. T. Davis, *AIChE J*., **26**, 705 (1980).
39. T. Lafitte, B. Mendiboure, M. M. Pineiro, D. Bessières and C. Miqueu, *J. Phys. Chem. B*., **114**, 11110 (2010).
40. A. Mejıa, I. Polishuk, H. Segura and J. Wisniak, *Thermochim. Acta*, **411**, 171 (2001).
41. A. Mejıa, H. Segura, L. F. Vega and J. Wisniak, *Fluid Phase Equilib*., **227**, 225 (2005).
42. C. Miqueu, J. M. Migues, M. M. Pineiro, T. Lafitte and B. Mendiboure, *J. Phys. Chem. B*., **115**, 9618 (2011).
43. M. Sahimi and B. N. Taylor, *J. Chem. Phys*., **95**, 6749 (1991).
44. C. Miqueu, B. Mendiboure, C. Graciaa and J. Lachaise, *Fluid Phase Equilib*., **218**, 189 (2004).
45. V. Bongiorno, L. E. Scriven and H. T. Davis, *J. Colloid Interface Sci*., **57**, 462 (1976).
46. Y. X. Zuo and E. H. Stenby, *In Situ*., **22**, 157 (1998).
47. Y. X. Zuo and E. H. Stenby, *J. Colloid Interface Sci*., **182**, 126 (1996).
48. M. B. Oliveira, I. M. Marrucho, J. A. P. Coutinho and A. J. Queimada, *Fluid Phase Equilib*., **267**, 83 (2008).
49. G. M. Kontogeorgis, I. V. Yakoumis, H. Meijer, E. Hendriks and T. Moorwood, *Fluid Phase Equilib*., **160**, 201 (1999).
50. H. Haghighi, *Phase equilibria modelling of petroleum reservoir fluids containing water*, Hydrate Inhibitors and Electrolyte Solutions, Ph.D. Thesis, University of Heriot-Watt, Institute of Petroleum Engineering (2009).
51. V. G. Baidakov, K. V. Khvostov and G. N. Muratov, *Zh. Fiz. Khim*., **56**, 814 (1982).
52. Q.-Y. Ren, G.-J. Chen, W. Yan and T.-M. Guo, *J. Chem. Eng. Data*, **45**, 610 (2000).
53. W. Yan, G.-Y. Zhao, G.-J. Chen and T. M. Guo, *J. Chem. Eng. Data*, **46**, 1544 (2001).
54. A. Georgiadis, G. Maitland, J. P. M. Trusler and A. Bismarck, *J. Chem. Eng. Data*, **55,** 4168 (2010).